A Monograph Pasticcio on the Mathematical and Engineering Background to the Leeming Awning

1. Abstract

The focus of this work is the appropriate combination of different physical and numerical disciplines to account for the relevant factors inherent to the design of a lightweight membrane structure. The scope of the work encompasses numerical form finding of tensile structures, computation of dynamic stresses and deformations of the initial structures under various tensile loads, and the modelling of wind flow in a neutrally stratified Atmospheric Boundary Layer. In this way various wind induced aeroelastic loadings and deformations on the structure (the Leeming Awning) can be derived.

Acknowledgements

This work owes its entire existence to the following:-

The mathematicians of Nizhny Novgorod State University, Russia,
Dr. Alexander Markus Kupzok of Technische Universität München, Munich, Germany,
Dr. Ren Schibo of Delft University of Technology, Netherlands,
Prof. Ruy Marcelo de Oliveira Pauletti, Polytechnic School of the University of São Paulo, Brazil

"We stand on the shoulders of giants"

Aitken	Ekman	Kirchhoff	Navier	Seidel
Allmaras	Euler	Kolmogorov	Neumann	Smagorinsky
Bletzinger	Galerkin	Kronecker	Newmark	Spalart
Boltzmann	Gauss	Krylov	Newton	St.Venant
Boussinesq	Green	Lagrange	Piola	Stokes
Bubnov	Hadamard	Lamé	Poisson	Taylor
Cauchy	Hellinger	Lattice	Prandl	Von-Mises
Dirichlet	Hooke	Leibnitz	Raphson	Washizu
Ehrhard	Hu	Mach	Reissner	Weibull
Einstein	Kàrmàn	Menter	Reynolds	

2. Structural Modeling of the Leeming Awning

The Leeming Awning is a bespoke tensile structure designed to be quickly attached to the front of a 17th century cottage to provide rain protection and shading. Structural modeling is based on Finite Element Analysis (FEA). Starting from the basics of continuum mechanics and introducing methods of space and time discretisation, the formulation for a generic hexahedral 3-dimensional Finite Element is derived and then used.

For the modeling of membrane structures, a special type of Finite Element is based on this generic hexahedral element. Usually, membrane structures used in civil engineering are prestressed. The consideration of this prestress state requires experimental or computational techniques, commonly referred to as form finding procedures, which are briefly introduced.

All the techniques presented in this pasticcio are applied to set up the structural model of the Leeming Awning mobile canopy structure. In later works, this model is used for further analysis with respect to wind loading, both on a rigid structure and with taking into account aero-elastic effects using methods of Fluid-Structure Interaction.

2.1 Characteristics of Membrane Structures

Shape and physical behavior of fabric structures is very different to those of conventional constructions based on stiff frames. These differences result from the missing bending stiffness of membrane material. Without the possibility of load transfer via bending action, the whole load transfer has to be carried out through stress acting tangential to the membrane surface. This tangential acting stress is referred to as membrane stress. The membrane is able to carry tension stress only. Compression in the membrane leads to a phenomenon of structural instability vis. the occurrence of wrinkles.

Due to the fact that the distribution of the tangential stress over the membrane thickness is constant, the utilisation of material strength is optimal. However, a strong interaction between shape and structural behavior occurs. In a static configuration the tangential tension stresses of the membrane are in equilibrium at every point. If this equilibrium is disturbed, e.g. by an external load, the membrane will react with deformations in such a way that the internal membrane stress and the external loading reach a new state of equilibrium. For loads acting perpendicularly to the membrane surface this usually results in large deformations.

The sensitivity of membrane structures with respect to external loadings is determined by their stiffness. This stiffness is mainly a result of two factors: geometry and prestress.

For distributed loads acting not only tangential to the surface, including dead load of

the membrane material, the geometry of the membrane needs to be curved in order to enable equilibrium between internal membrane stress and loading. These double curved surfaces can be classified as synclastic or anticlastic, depending on the sign of their Gaussian curvature.

Prestress is introduced in membrane structures to provide the flexible fabric with an additional geometric stiffness and ensure that for all load cases no compressive stress occurs. The initial geometry of the prestress membrane is the shape, for which the membrane forces introduced by the prestress and those due to dead load are in equilibrium. In general, this shape is unknown and form-finding procedures are used to determine the initial shape. These can be conducted as experiments or by numerical computations, the form-finding computations.

For membrane structures, the prestress is realised as mechanical or pneumatic prestress. Since prestress can only be imposed as tension, it is also known as pretension.

a **Pneumatically imposed prestress**

Pneumatically imposed prestress is caused by a pressure difference between both sides of the membrane. This leads to overall synclastic shapes with positive Gaussian curvature, such as balloons or cushions. Air supported structures, usually in the form of shallow spherical 'caps' are another typical application. Fig. 2.1 provides examples of synclastic, pneumatically prestressed constructions.

(a) Balloon shape. (b) Cushion shape.

Figure 2.1: Generic synclastic shapes.

b **Mechanically imposed prestress**

Mechanically imposed prestress is introduced by tightening the anchorage. Typically, the geometries for mechanically prestressed structures are anticlastic, meaning the sign of their Gaussian curvature is negative. In fig. 2.2 the four generic types of anticlastic surfaces are presented: cone, saddle-surface, hyperboloid and "ridge and valley".

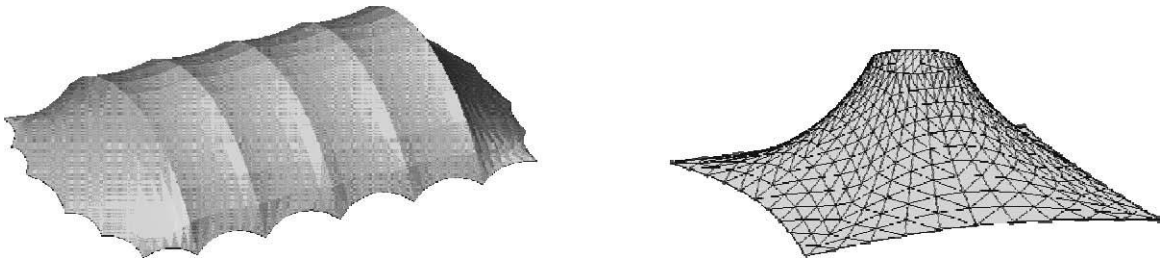

(a) Saddle shape. (b) Cone shape.

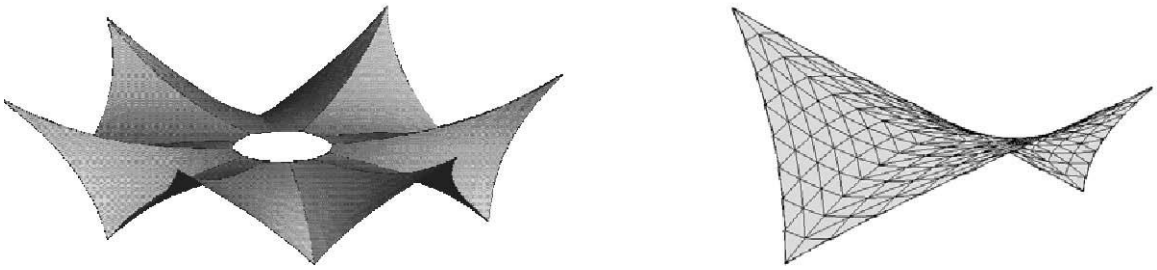

(c) 'Ridge & valley' shape. (d) Hyperboloid shape.

Figure 2.2: Generic anticlastic shapes.

In the following, only mechanically prestressed structures shall be considered.

Prestressed membrane structures commonly require continuous support along the edges to maintain a prestressed state. This support can be rigid, such as a stiff beam or anchorage or, more commonly, flexible. Flexible support is realised by cables attached to the edges of the membrane. They are curved due to the (pre-)tension stress of the membrane and, therefore, also subject to (pre-)tension. If the stress at the edges of the membrane acts tangential to the edge cables, the membrane might slide along the cable, which is usually prevented by additional fittings.

For the realisation of membrane structures, a variety of synthetic materials with different properties are available. They can be categorised into two groups: fabrics and foils.

a **Fabrics**

Fabrics show an anisotropic behavior in the directions of their fibres. Corresponding to the manufacturing process of fabrics, the two directions are called warp and weft. The fabric determines the load carrying behavior. Commonly a coating is applied which protects the fibers from mechanical, chemical, or biological damage and determines the transparency and sealing. Typical examples for these composite materials are PVC (Polyvinylchloride) coated polyester fabrics or PTFE (Polytetrafluoroethylene) coated glass fiber fabrics.

b **Foils**

Foils have an isotropic material behavior. A typical material for foil constructions in civil engineering is ETFE (Ethylentetrafluoroethylene). ETFE is highly transparent, has a high chemical resistance and a penetrability towards air that is small enough for the usage in pneumatic structures. Compared to fabric materials of the same thickness, foils typically have a lower load carrying capacity. Therefore, foil structures

usually have a limited free span.

2.2 Fundamentals of Structural Analysis

2.2.1 Fundamentals of Continuum Mechanics

In the following, a brief introduction to the field of continuum mechanics is given. The presented explanations are restricted to those most relevant to the topic of light-weight structures.

2.2.1.1 Differential Geometry

A material point **M** of a continuous body B in a three dimensional space can be identified by its position vector $\mathbf{x}(\theta^1, \theta^2, \theta^3)$. The position vector refers to curvilinear convective coordinates θ^i (fig. 2.3). In the following, the summation convention by Einstein will be used. Latin indices take values 1 to 3, while Greek indices take values 1 and 2. The base vectors of the curvilinear coordinate system θ^i can be derived as:

$$\mathbf{g_i} = \frac{\partial \mathbf{x}}{\partial \theta^i} \tag{2.1}$$

The elements $\mathbf{g_i}$ are called covariant base vectors. Additional to the covariant basis, a reciprocal (or dual) basis is introduced. The elements of the reciprocal basis are called contravariant base vectors $\mathbf{g^i}$. The two bases $\mathbf{g_i}$ and $\mathbf{g^i}$ satisfy the following condition:

$$\mathbf{g_i} \cdot \mathbf{g^j} = \delta^i_j \tag{2.2}$$

δ^i_j is the (mixed) Kronecker delta. Based on the curvilinear coordinate system θ^i the contravariant base vectors can be derived by the following equation:

$$\mathbf{g^i} = \frac{\partial \theta^i}{\partial \mathbf{x}} \tag{2.3}$$

By using the scalar product on two covariant base vectors, the metric coefficients g_{ij} of the covariant basis are calculated. Same holds for the contravariant base vector and the metric coefficients g^{ij} of the contravariant basis:

$$g_{ij} = \mathbf{g_i} \cdot \mathbf{g_j} \qquad g^{ij} = \mathbf{g^i} \cdot \mathbf{g^j} \tag{2.4}$$

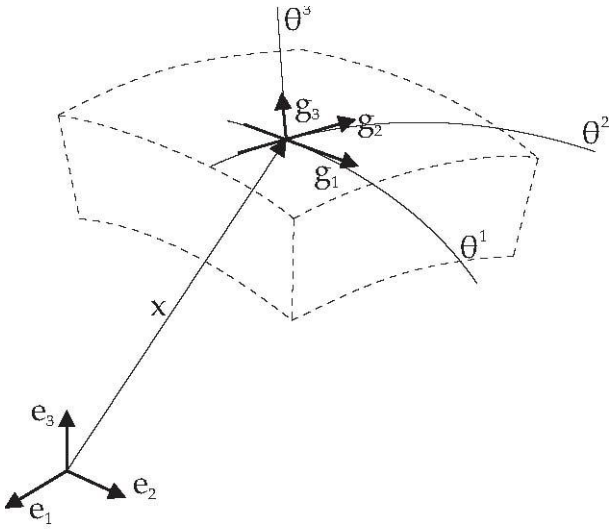

Figure 2.3: Geometry in curvilinear coordinates.

The Unity (or Identity) tensor or Metric tensor of a coordinate system is derived as:

$$\mathbf{I} = g_{ij}\mathbf{g}^{i}(\quad I = g_{ij}\, g^{i} \otimes g^{j} = g^{ij}\, g_{i} \otimes g_{j} = g_{i} \otimes g^{j} = g^{i} \otimes g_{j} \qquad (2.5)$$

with $\otimes$ as the dyadic product.

2.2.1.2 Kinematics

For each material point **M** of a continuum body B the mapping κ assigns a position **x** at a certain time *t*. The configuration at a defined time $t=t_0$ is called the reference configuration and is the initial configuration of the system. Configurations for $t>t_0$ are called current configurations. In the following, all quantities based on the reference configuration are expressed in upper case letters, while those based on current configurations are expressed in lower case letters.

The motion χ is defined as the transformation from reference to current position at a time *t*:

$$\mathbf{x} = \chi(\mathbf{X}, t) \qquad (2.6)$$

Commonly, in structural mechanics, a Lagrangian description is used, in which the coordinate system "sticks" to a material point and changes, when the position of the material point is modified. Therefore, a material point is identified by its Lagrange coordinates $\mathbf{X}(\theta^1, \theta^2, \theta^3)$

and the point in time *t*. The displacement field **d** from reference to current configuration can be expressed as:

$$\mathbf{d}(\mathbf{X}, t)=\chi(\mathbf{X}, t)-\mathbf{X} =\mathbf{x}(\mathbf{X}, t)-\mathbf{X} \qquad (2.7)$$

According to the definition of the co-and contravariant base vectors in the current configuration ($\mathbf{g}_i$ and $\mathbf{g}^i$) at a position $\mathbf{x}(\theta^1, \theta^2, \theta^3)$ (eq. 2.1 and eq. 2.3), the co-and contravariant base vectors of reference configuration at a position $\mathbf{X}(\theta^1, \theta^2, \theta^3)$ are:

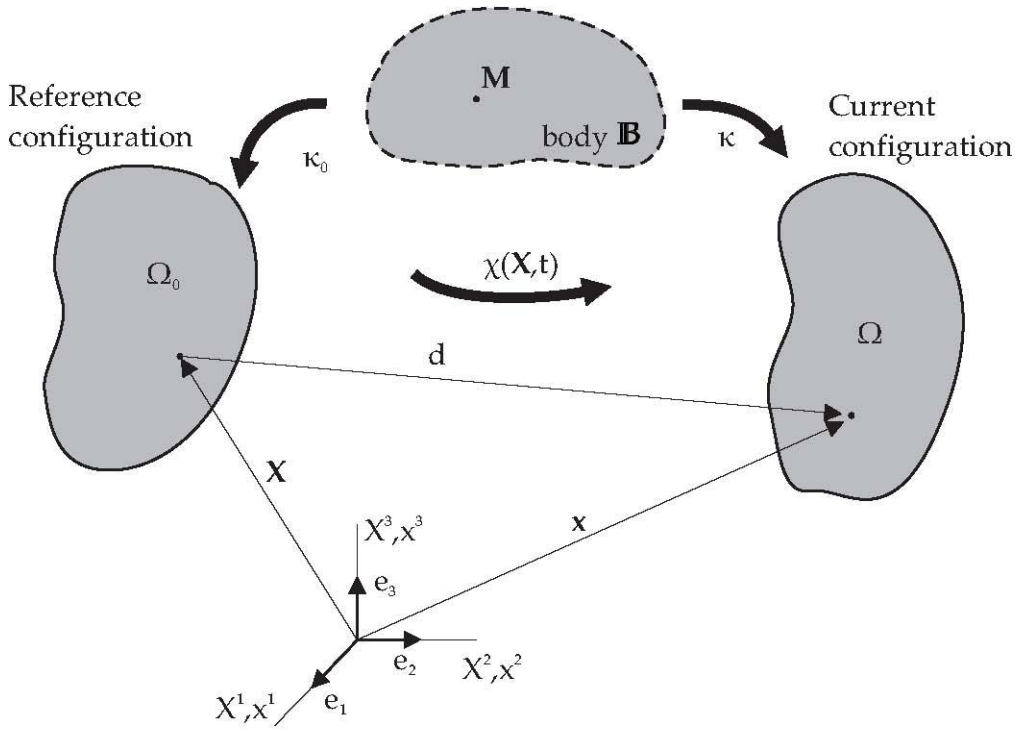

Figure 2.4: Configuration and motion of a continuum body and a material point.

$$G_i = \frac{\partial X}{\partial \theta^i} \qquad G^i = \frac{\partial \theta^i}{\partial X} \qquad (2.8)$$

The material deformation gradient **F** describes the mapping of a differential line element in the reference configuration $d\mathbf{X} =\mathbf{G}_i d\theta^i$ into a line element in the deformed configuration $d\mathbf{x} =\mathbf{g}_i\, d\theta^i$:

$$dx = \frac{\partial x}{\partial X} dX = F \cdot dX \qquad (2.9)$$

Commonly, **F** is an asymmetric second order tensor. As the mapping of a line element is equivalent to the mapping of a base vector from reference to current configuration the de-

formation gradient can be used to relate co-and contravariant base vectors in reference and current configuration:

$$\mathbf{g_i} = \mathbf{F} \cdot \mathbf{G_i} \quad \mathbf{g^i} = \mathbf{F}^{-T} \cdot \mathbf{G^i} \qquad \mathbf{G_i} = \mathbf{F}^{-1} \cdot \mathbf{g_i} \qquad \mathbf{G^i} = \mathbf{F}^{T} \cdot \mathbf{g}^{I} \tag{2.10}$$

Accordingly, **F** can be derived as:

$$\mathrm{F} = \frac{\partial \mathrm{x}}{\partial \mathrm{X}} = g_I \otimes G^I \qquad \mathrm{F}^{\mathrm{T}} = G^I \otimes g_I \neq \mathrm{F} \qquad \mathrm{F}^{-\mathrm{T}} = g^I \otimes G_I \qquad \mathrm{F}^{-1} = G_I \otimes g^I \tag{2.11}$$

The deformation gradient contains information about the complete deformation process, including rigid body deformations. Therefore, it is not objective and cannot be used directly as a strain measure. Instead, the objective, symmetric Green-Lagrange (**GL**) strain tensor **E** is introduced for the description of large displacements (with **I** as the identity tensor):

$$\mathrm{E} = \frac{1}{2}(\mathrm{F}^{\mathrm{T}}\mathrm{F} - \mathrm{I}) = E_{IJ}\, \mathrm{G}^{\mathrm{i}} \otimes \mathrm{G}^{\mathrm{j}} = \frac{1}{2}(g_{IJ} - G_{IJ})\mathrm{G}^{\mathrm{i}} \otimes \mathrm{G}^{\mathrm{j}} \tag{2.12}$$

2.2.1.3 Constitutive Equations

The constitutive equation describes the connection between static and kinematic quantities, thus between stress and strains. The energetically conjugate quality for the Green-Lagrange (**GL**) strain tensor **E** is the symmetric second Piola-Kirchhoff (**PK2**) stress tensor **S**.

GL strain tensor and PK2 stress tensor are used to compute the internal energy of a deformed body. The property of orthogonality of the co-and contravariant metrics are used to ensure that the internal energy is independent of the used metric: the strain tensor is based on the covariant, while the stress tensor is based on the contravariant basis. The PK2 stress tensor is based in the reference configuration and has no physical meaning. A measurement for the real physical stress is the symmetric Cauchy stress tensor σ:

$$\sigma = \sigma^{ij}\mathrm{g_i} \otimes \mathrm{g_i} \tag{2.13}$$

With the use of the deformation gradient, the PK2 stress tensor can be transformed into the Cauchy stress tensor and vice versa:

$$\sigma = (\det\mathbf{F})^{-1}\mathbf{F}\mathbf{S}\mathbf{F}^{T} \qquad \mathbf{S} = \det\mathbf{F}\,\mathbf{F}^{-1}\sigma\mathbf{F}^{-T} \tag{2.14}$$

In the scope of this work, large deformations with small strains are analyzed. The St. Venant-Kirchhoff material law is used, which is a generalisation of the linear elastic Hooke's material law for large rotations. Using the strain energy density $W^{int}(\mathbf{E})$, the constitutive relation can be formulated as:

$$\mathrm{S} = \frac{\partial \mathrm{W}^{\mathrm{int}}(\mathrm{E})}{\partial \mathrm{E}} \tag{2.15}$$

The fourth order elasticity tensor C is derived by linearising the constitutive relation:

$$\mathrm{C} = \frac{\partial \mathrm{S}}{\partial \mathrm{E}} \quad \text{with} \quad \mathrm{C} = C^{ijkl}\mathrm{G}_i \otimes \mathrm{G}_j \otimes \mathrm{G}_k \otimes \mathrm{G}_l \tag{2.16}$$

∂**E** and describes a linear relation between the GL strain tensor **E** and the PK2 **S** stress tensor:

$$\mathrm{S} = \mathbb{C} : \mathrm{E} \quad \text{with} \quad S^{ij} = C^{ijkl}E_{kl} \tag{2.17}$$

The general elasticity tensor has 3^4 =81 independent coefficients, which can be reduced to 36 due to the symmetry of the PK2 stress and GL strain tensors. For an isotropic material, two parameters are sufficient to describe the material properties. In a mathematical context usually the Lamé constants λ and μ are used, while in an engineering context Young's modulus E and Poisson's ratio ν are applied.

$$\lambda = \frac{E\nu}{(1+\nu)(1-2\nu)} \qquad \mu = \frac{E}{2(1+\nu)} \tag{2.18}$$

Using the Lamé constants, the components of the elasticity tensor for an isotropic material can be determined by:

$$C^{ijkl} = \lambda G^{ij}G^{kl} + \mu[G^{ik}G^{jl} + G^{il}G^{kj}] \tag{2.19}$$

2.2.1.4 Equilibrium Conditions

Within this work, no velocity dependent physical damping is considered. The momentum balance principle states that inner forces, inertia forces, external forces, and body forces acting on a body and its surface have to be in equilibrium. In the current configuration, this equilibrium is expressed in eq. 2.20, which is known as Cauchy's first equation of motion.

$$\int_{\Omega} (\nabla \cdot \sigma + \mathrm{b} - \rho \ddot{\mathrm{d}}) d\Omega = 0 \tag{2.20}$$

In the reference configuration, the momentum balance principle is formulated as:

$$\int_{\Omega_0} (\nabla \cdot \mathrm{P} + \mathrm{B} - \rho_0 \ddot{\mathrm{d}}) d\Omega_0 = 0 \tag{2.21}$$

B and b are vectors of body forces per volume unit, acting in the reference and current configuration respectively. The acceleration field **d** is the second derivative of the displacement field with respect to time. **P** is the first Piola Kirchhoff (**PK1**) stress tensor, which is asymmetric and defined in both, the current and the reference configuration. Therefore, it is advantageous to exchange it for the PK2 stress tensor using eq. 2.22.

$$\mathbf{P} = \mathbf{FS} \tag{2.22}$$

The equation of motion expressed with the PK2 stress tensor is the following:

$$\int_{\Omega_0} (\nabla \cdot (\mathrm{F}\,\mathrm{S}) + \mathrm{B} - \rho_0 \ddot{\mathrm{d}}) d\Omega_0 = 0 \tag{2.23}$$

Since the equation of motion has to be fulfilled for every domain Ω_0 it can be transferred into a local perspective:

$$\nabla \cdot (\mathbf{FS}) + \mathbf{B} - \rho_0 \ddot{\mathbf{d}} = \mathbf{0} \tag{2.24}$$

Together with appropriate initial conditions and boundary conditions, eq. 2.12, eq. 2.17, and eq. 2.24 present the strong form of the elastic dynamic boundary value problem in material description. It is a system of nonlinear coupled hyperbolic partial differential equations. The initial conditions describe position, state of deformation, and state of motion at the initial point in time. Therefore, the displacement field $\mathbf{d} = \mathbf{d}_0$ and the velocity field $\dot{\mathbf{d}} = \dot{\mathbf{d}}_0$ are to be prescribed at time $t = t_0$ for the whole domain Ω_0.

The boundary conditions on the body surface Γ consist of the Dirichlet boundary condition Γ_D, which specifies a prescribed deformation $\hat{d}$ of the boundary surface and the Neumann boundary condition Γ_N, which specifies a prescribed force vector $\hat{\mathbf{T}}_\mathbf{N}$ on the boundary.

$$\begin{aligned} d &= \hat{d} \quad \text{for} \quad \Gamma_D \quad \forall\, t \in [t_0, T] \\ \mathrm{T} &= \hat{\mathrm{T}}_\mathrm{N} \quad \text{for} \quad \Gamma_N \quad \forall\, t \in [t_0, T] \end{aligned} \tag{2.25}$$

At a specific point of the boundary for a specific degree of freedom, either a Dirichlet or a Neumann boundary condition can be prescribed:

$$\Gamma_N \cap \Gamma_D = 0 \quad \text{with} \quad \Gamma = \Gamma_N \cup \Gamma_D \tag{2.26}$$

2.2.1.5 The Weak Form -the Principle of Virtual Work

For two-or three-dimensional problems, an exact solution of elastic dynamic boundary value problem is in general not possible. In the scope of this work, the well established

Finite Element Method is used to solve problems of structural mechanics.

The Finite Element Method is based on variational principles and provides a solution technique in which selected field equations and selected boundary conditions are satisfied in integral form. In contrast to the original differential equation, in the integral formulation the requirements for differentiability of the solution functions are weaker. Therefore, the integral form is referred to as the weak form, whereas the original differential equation is referred to as the strong form of the problem.

The most basic and common variational principle is the principle of virtual work. It is the basis of standard Galerkin finite element models. Using the principle of virtual work, the equilibrium condition and the traction boundary conditions are not exactly satisfied but are approximated in an integral sense. The kinematic equation and the material law are represented exactly.

To derive the principle of virtual work, the first Cauchy equation of motion and the Neumann boundary conditions are multiplied by an arbitrary test function and integrated over the volume of the domain Ω_0. The test function is chosen as a variation of the displacement field $\delta\mathbf{d}$. This virtual displacement field can be arbitrary but has to be compatible to the Dirichlet boundary conditions. By multiplication of the equation of motion and the Neumann boundary conditions with a virtual displacement field, the existence of a virtual work is assumed. In a state of equilibrium, the virtual work δW, that is performed by the internal and external forces of the system due to the virtual displacement field shall be zero.

$$\delta W = \delta W_{dyn} + \delta W_{int} - \delta W_{ext} = 0 \qquad (2.27)$$

The virtual work δW can be separated in contributions due to inertia forces δW_{dyn}, internal forces δW_{int}, and external forces δW_{ext}.

$$\delta W_{dyn} = \int_{\Omega_0} \rho_0 \ddot{\mathbf{d}} \cdot \delta\mathbf{d} \, d\Omega_0 \qquad (2.28)$$

$$\delta W_{int} = \int_{\Omega_0} \delta\mathbf{E} : \mathbf{S} \, d\Omega_0 \qquad (2.29)$$

$$\delta W_{ext} = \int_{\Gamma_0} \bar{\mathbf{T}} \cdot \delta\mathbf{d} \, d\Gamma_0 + \int_{\Omega_0} \rho_0 \mathbf{B} \cdot \delta\mathbf{d} \, d\Omega_0 \qquad (2.30)$$

Equation 2.29 contains the expression of virtual strain $\delta\mathbf{E}$. $\delta\mathbf{E}$ is related to the virtual displacement $\delta\mathbf{d}$ by the following relations:

$$\delta\mathbf{E} = \frac{1}{2}(\delta\mathbf{F}^{\mathrm{T}} \cdot \mathbf{F} + \mathbf{F}^{\mathrm{T}} \cdot \delta\mathbf{F}) \qquad (2.31)$$

with

$$\mathbf{F} = \mathbf{I} + \frac{\partial \mathbf{d}}{\partial \mathbf{X}} \quad \text{and} \quad \delta\mathbf{F} = \frac{\partial(\delta\mathbf{d})}{\partial \mathbf{X}}$$

(2.32)

Inserting eq. 2.28, eq. 2.29, eq. 2.30 into eq. 2.27, the weak form of the boundary value problem of nonlinear elastic dynamics based on the principle of the virtual work is formulated:

$$\delta W = \int_{\Omega_0} \rho_0 \ddot{\mathbf{d}} \cdot \delta \mathbf{d} \, d\Omega_0 + \int_{\Omega_0} \delta \mathbf{E} : \mathbf{S} \, d\Omega_0 - \int_{\Gamma_0} \bar{\mathbf{T}} \cdot \delta \mathbf{d} \, d\Gamma_0 - \int_{\Omega_0} \rho_0 \mathbf{B} \cdot \delta \mathbf{d} \, d\Omega_0 = 0 \qquad (2.33)$$

The principle of virtual work is equivalent to the field equations (eq. 2.12, eg. 2.17, and eq. 2.24), as long as the same function spaces are used to solve both system of equations. For the derivation of the principle of virtual work, only the variation of the displacement is performed. There is a practically infinite multitude of alternative variational formulations, containing all possible combinations of weak and strong satisfaction of the field equations and boundary conditions, as well as additional variants that can be obtained by weighted combinations of these basic principles ("parameterized variational principles"). Next to the principle of virtual displacement the most important principles are the Hellinger-Reissner principle and the Hu-Washizu principle. Table 2.1 gives a brief comparison between the most important variational principles in context of the finite element method.

principle	variables	Euler-Lagrange equations (weakly satisfied)	subsidiary conditions strongly satisfied
virtual work	$\mathbf{d}$	equilibrium traction boundary conditions	kinematic equation material law displacement boundary cond.
Hellinger-Reissner	$\mathbf{d}, \sigma$	equilibrium kinematic equation traction boundary cond. displacement boundary cond.	material law
Hu-Washizu	$\mathbf{d}, \sigma, \epsilon$	equilibrium kinematic equation material law traction boundary cond. displacement boundary cond.	

Table 2.1: Comparison of variational principles

2.2.2 Numerical Modeling

In order to apply the Finite Element Method, the continuous formulation of the boundary value problem of nonlinear elasto-dynamics has to be transformed into a discretised form. Starting from the weak form (eq. 2.33), a time and space wise discretisation is conducted. This leads to a non-linear system of equations, which can be solved conveniently in an iterative manner using computer resources. The following sections introduce the fundamental ideas and methods of space and time integration. Further information about the specific element formulations used in the scope of this work are presented in section 2.3.1.

2.2.2.1 Space Discretisation

A continuous body **B** is divided into non-overlapping domains Ω_e, the so-called finite elements (eq. 2.34). The quantities of the considered problem, such as displacements or stress, are specified by element wise functions within the finite elements. Thereby, the relevant continuous quantities are transferred to a discrete set of unknowns and thus approximated on a local level.

$$\mathrm{B} \approx \mathrm{B}^h = \bigcup_{e=1}^{n_{ele}} \Omega_e \tag{2.34}$$

In the following, the formulation of a basic three-dimensional brick element shall be derived.

For a finite element Ω_e, the shape functions $N_i(\xi, \eta, \mu)$ for all nodes i of the element are described by the natural coordinates ξ, η, and μ as parameters. The position vector of the reference and the current configuration of a point can be described as:

$$\mathrm{X} \approx \mathrm{X}^h(\xi,\eta,\mu) = \sum_{I=1}^{n_{nod}} N_I(\xi,\eta,\mu) \cdot \overline{\mathrm{X}}_\mathrm{I} \tag{2.35}$$

$$\mathrm{x} \approx \mathrm{x}^h(\xi,\eta,\mu) = \sum_{I=1}^{n_{nod}} N_I(\xi,\eta,\mu) \cdot \overline{\mathrm{x}}_\mathrm{I} \tag{2.36}$$

The superscript h indicates an approximated quantity. n_{nod} is the number of nodes within the finite element. Assuming that the position vectors of the nodes ($\mathbf{X_i}$, $\mathbf{x}_i$) refer to the global Cartesian base, the parameters ξ, η, μ can be identified as the coordinates θ^1, θ^2, θ^3. The same coordinates were used in section 2.2.1.1 for the description of the differential geometry. Considering eq. 2.7, the displacement field can be approximated to:

$$\begin{aligned} \mathrm{d}(\theta^1,\theta^2,\theta^3) \approx \mathrm{d}^h(\theta^1,\theta^2,\theta^3) &= \mathrm{x}^h(\theta^1,\theta^2,\theta^3) - \mathrm{X}^h(\theta^1,\theta^2,\theta^3) \\ &= \sum_{I=1}^{n_{nod}} N_I(\theta^1,\theta^2,\theta^3) \cdot (\overline{\mathrm{x}}_\mathrm{I} - \overline{\mathrm{X}}_\mathrm{I}) \\ &= \sum_{I=1}^{n_{nod}} N_I(\theta^1,\theta^2,\theta^3) \cdot \overline{\mathrm{d}}_\mathrm{I} \end{aligned} \tag{2.37}$$

Comparing eq. 2.35, eq. 2.36,

and eq. 2.37 it becomes obvious that the same set of shape functions N_i can be used to approximate both: geometry and displacements. This duality in element formulations is known as the iso-parametric concept. As the shape functions are time independent, velocity and acceleration can be derived in eq. 2.38 and eq. 2.39 in discretized form:

$$\dot{\mathbf{d}}^h(\theta^1,\theta^2,\theta^3) = \sum_{i=1}^{n_{nod}} N_i(\theta^1,\theta^2,\theta^3) \cdot \dot{\overline{\mathbf{d}}}_\mathbf{i} \tag{2.38}$$

$$\ddot{\mathbf{d}}^h(\theta^1,\theta^2,\theta^3) = \sum_{i=1}^{n_{nod}} N_i(\theta^1,\theta^2,\theta^3) \cdot \ddot{\overline{\mathbf{d}}}_\mathbf{i} \tag{2.39}$$

Accordingly, with eq. 2.2 and eq. 2.3, the covariant base vectors of the discretized geometry for reference and current configuration are:

$$\mathbf{G}_I^h = \mathbf{X}^h{}_{,I} = \frac{\partial \mathbf{X}^h}{\partial \theta^I} = \sum_{i=1}^{n_{nod}} N_i(\theta^1,\theta^2,\theta^3)_{,I} \cdot \overline{\mathbf{X}}_i \tag{2.40}$$

$$\mathbf{g}_I^h = \mathbf{x}^h{}_{,I} = \frac{\partial \mathbf{x}^h}{\partial \theta^I} = \sum_{i=1}^{n_{nod}} N_i(\theta^1,\theta^2,\theta^3)_{,I} \cdot \overline{\mathbf{x}}_i \tag{2.41}$$

Using eq. 2.40 and eq. 2.41 in combination with eq. 2.11 the discretized deformation gradient and, via eq. 2.12, the discretized Green-Lagrange strain tensor is formulated.

The Bubnov-Galerkin method that is applied here uses the same interpolation concept for real quantities of the problem as for assumed test or virtual quantities. The variation of the displacement in the discretized form, according to eq. 2.37, is:

$$\delta\mathbf{d}^h(\theta^1,\theta^2,\theta^3) = \sum_{i=1}^{n_{nod}} N_i(\theta^1,\theta^2,\theta^3) \cdot \delta\overline{\mathbf{d}}_\mathbf{i} \tag{2.42}$$

As the geometry is discretized into non-overlapping finite domains, so-called elements, the principle of virtual work can be expressed on an element level. The integration is performed numerically by applying the Gauss quadrature rule in an element wise manner. Therefore, element based, local coordinate systems are introduced. The change of base from the physical curvilinear coordinate system to the element wise local system has to be incorporated into the integration.

In the following, element based quantities are indicated by the superscript *e*. The contributions of virtual work on all elements sum up to the virtual work of the whole system:

$$\delta W^h = \delta W^h_{dyn} + \delta W^h_{int} - \delta W^h_{ext} = \sum_{e=1}^{n_{ele}} \delta W^e_{dyn} + \sum_{e=1}^{n_{ele}} \delta W^e_{int} - \sum_{e=1}^{n_{ele}} \delta W^e_{ext} \tag{2.43}$$

For the discretisation of the virtual work due to forces of inertia, the approximations introduced in eq. 2.39 and eq. 2.42 are used. The contribution of one element is:

$$\delta W^e_{dyn} = \int_{\Omega^e_0} \rho_0 \, \delta \mathbf{d}^h \cdot \ddot{\mathbf{d}}^h \, d\Omega^e_0 \tag{2.44}$$

$$= \int_{\Omega^e_0} \rho_0 \left(\sum_{i=1}^{n_{nod}} N_i(\theta^1,\theta^2,\theta^3) \cdot \delta \bar{\mathbf{d}}_i \right) \left(\sum_{j=1}^{n_{nod}} N_j(\theta^1,\theta^2,\theta^3) \cdot \ddot{\bar{\mathbf{d}}}_j \right) d\Omega^e_0 \tag{2.45}$$

$$= \sum_{i=1}^{n_{nod}} \sum_{j=1}^{n_{nod}} \delta \bar{\mathbf{d}}_i \cdot \underbrace{\left[\int_{\Omega^e_0} \rho_0 \, N_i(\theta^1,\theta^2,\theta^3) \, N_j(\theta^1,\theta^2,\theta^3) \, \mathrm{I} \, d\Omega^e_0 \right]}_{\mathbf{m}^{e\,ij}} \cdot \ddot{\bar{\mathbf{d}}}_j \tag{2.46}$$

$$= \sum_{i=1}^{n_{nod}} \sum_{j=1}^{n_{nod}} \delta \bar{\mathbf{d}}_i \cdot \mathbf{m}^{e\,ij} \cdot \ddot{\bar{\mathbf{d}}}_j \tag{2.47}$$

Summarising the nodal degrees of freedom within one element to a vector $\bar{\mathbf{d}}^e$, the mass matrix of an element can be correspondingly expressed as $\mathbf{m}^e$. Using this notation, the contribution of the forces of inertia to the virtual work can be written as:

$$\delta W^e_{dyn} = \delta \bar{\mathbf{d}}^{eT} \mathbf{m}^e \ddot{\bar{\mathbf{d}}}^e \tag{2.48}$$

For distributed, non-constant external loading on the boundary, the consistent nodal load vector is derived by integration of the load over the element surface using the shape function. In the following, it is assumed, that external loads and body forces are independent of the deformation of the structure: $\mathbf{T}^h_{,\mathbf{d}} = \mathbf{0}$ and $\mathbf{B}^h_{,\mathbf{d}} = \mathbf{0}$.

$$\delta W^e_{ext} = \int_{\Gamma^e_0} \hat{\mathbf{T}} \cdot \delta \mathbf{d}^h \, d\Gamma^e_0 + \int_{\Omega^e_0} \rho_0 \, \mathrm{B} \cdot \delta \mathbf{d}^h \, d\Omega^e_0 \tag{2.49}$$

$$= \int_{\Gamma^e_0} \hat{\mathbf{T}} \cdot \left(\sum_{i=1}^{n_{nod}} N_i(\theta^1,\theta^2,\theta^3) \cdot \delta \bar{\mathbf{d}}_i \right) d\Gamma^e_0 + \int_{\Omega^e_0} \rho_0 \, \mathrm{B} \cdot \left(\sum_{i=1}^{n_{nod}} N_i(\theta^1,\theta^2,\theta^3) \cdot \delta \bar{\mathbf{d}}_i \right) d\Omega^e_0 \tag{2.50}$$

$$= \sum_{i=1}^{n_{nod}} \delta \bar{\mathbf{d}}_i \cdot \left[\int_{\Gamma^e_0} \hat{\mathbf{T}} \cdot N_i(\theta^1,\theta^2,\theta^3) \, d\Gamma^e_0 + \int_{\Omega^e_0} \rho_0 \, \mathrm{B} \cdot N_i(\theta^1,\theta^2,\theta^3) \, d\Omega^e_0 \right] \tag{2.51}$$

$$= \sum_{i=1}^{n_{nod}} \delta \bar{\mathbf{d}}_i \cdot \mathbf{r}^{e\,i}_{ext} \tag{2.52}$$

Integrating the contribution of the consistent nodal load vectors $\mathbf{r}^{ei}$ the load vector $\mathbf{r}^{e}$ is derived, which corresponds to the vector of unknown displacements $\mathbf{d}^{-e}$ of the problem. Assuming a time dependent load, the element load vector is $\mathbf{r}^{e}{}_{ext}(t)$. The discretized form of the virtual work due to time dependent external loading can be written as:

$$\delta W^e_{ext} = \delta \bar{\mathrm{d}}^e \mathbf{r}^e_{ext}(t) \tag{2.53}$$

The contribution of the internal forces is more difficult to be discretised due to the non-linearity of the Green-Lagrange strain tensor $\mathbf{E}(\bar{\mathbf{d}})$with respect to displacements $\bar{\mathbf{d}}$. The variation of the Green-Lagrange strain tensor is derived in a discretised form, using $\bar{\mathbf{d}}^{e}$ as a vector of the unknown displacements:

$$\frac{\partial \mathrm{E}^h(\bar{\mathrm{d}})}{\partial \bar{\mathrm{d}}^e}\,\delta\bar{\mathrm{d}}^e = \mathrm{E}^h{}_{,\bar{\mathrm{d}}^e}\;\delta\bar{\mathrm{d}}^e \tag{2.54}$$

Using this, the contribution of the internal forces can be transformed to:

$$\delta W^e_{int} = \int_{\Omega^e_0} \mathrm{S}^h : \delta \mathrm{E}^h \, d\Omega^e_0 = \int_{\Omega^e_0} \mathrm{S}^h : \mathrm{E}^h{}_{,\bar{\mathrm{d}}^e}\;\delta\bar{\mathrm{d}}^e \, d\Omega^e_0 \tag{2.55}$$

$$= \delta\bar{\mathrm{d}}^e \Big[\int_{\Omega^e_0} \mathrm{S}^h : \mathrm{E}^h{}_{,\bar{\mathrm{d}}^e}\; d\Omega^e_0\Big] = \sum_{I=1}^{n_{nod}} \delta\bar{\mathrm{d}}^e_I \cdot \mathrm{r}^{e\,I}_{int}(\bar{\mathrm{d}}) = \delta\bar{\mathrm{d}}^e \cdot \mathrm{r}^e_{int}(\bar{\mathrm{d}}) \tag{2.56}$$

Summarising the contributions of virtual work for one element, the spacial discretised equation of motion is derived.

$$\delta W^e = \delta W^e_{dyn} + \delta W^e_{int} - \delta W^e_{ext} = \delta\bar{\mathrm{d}}^e \cdot [\mathrm{m}^e\,\ddot{\bar{\mathrm{d}}}^e + \mathrm{r}^e_{int}(\bar{\mathrm{d}}) - \mathrm{r}^e_{ext}] = 0 \tag{2.57}$$

The virtual work for the whole system is deduced by assembling the contributions from each element according to 2.43:

$$\delta W = \delta W_{dyn} + \delta W_{int} - \delta W_{ext} = \delta\bar{\mathrm{d}} \cdot [\mathrm{M}\,\ddot{\bar{\mathrm{d}}} + \mathrm{r}_{int}(\bar{\mathrm{d}}) - \mathrm{r}_{ext}] = 0 \tag{2.58}$$

Correspondingly, $\mathbf{M}$ resembles the mass matrix of the system, which has to be computed only once due to the Lagrangian formulation. The vector $\bar{\mathbf{d}}$ contains all unknown degrees of freedom of the system. As well as its variation, the size and location of $\bar{\mathbf{d}}$ and its variation $\delta\bar{\mathbf{d}}$ have to comply with the Dirichlet boundary conditions.

Applying the fundamental lemma of variational calculus, the spacial discretised, nonlinear differential equation and the initial conditions are derived:

$$\mathrm{M}\,\ddot{\mathrm{d}} + \mathrm{r}_{int}(\mathrm{d}) = \mathrm{r}_{ext} \qquad \ddot{\mathrm{d}}(t = t_0) = \ddot{\mathrm{d}}_0, \qquad \dot{\mathrm{d}}(t = t_0) = \dot{\mathrm{d}}_0 \tag{2.59}$$

2.2.2.2 Time Discretisation

After the spacial discretisation in finite elements, eq. 2.59 states the semi-discrete problem. As the next step, time discretisation is performed. The continuous time period [t_0, This divided into n_t time steps of equal length Δt. The system quantities are not regarded as time wise continuous anymore, but as defined at discrete points in time t_n:

$$t_n = t_0 + \Delta t n \text{ with } n \in [0, n_t] \tag{2.60}$$

In a time integration scheme the system quantities at the end of the new time step t_{n+1} are computed based on those at the end of the previous time-steps t_n, t_{n-1}, t_{n-2}, etc. Time integration schemes can be classified into one-step and multi-step schemes, depending on the number of previous time steps used to derive the values for the new time step.

In explicit time integration schemes, the dynamic equilibrium based on the equation of motion is computed at the beginning of the time step. For implicit time integration schemes, the equilibrium is considered at the end of the time step. In an implicit scheme, the state of motion at the end of a time step depends on itself. Thus, for each time-step a system of equations has to be solved.

For the solution of problems concerning structural dynamics, implicit and explicit one-step time integration schemes have proven to be especially well suited . In the simulation of light-weight structures under wind loading, modes with relatively low frequencies are expected. Therefore, considerably large time step lengths are sufficient to capture the physically relevant responses. For the applicable time step length, stability issues of the time integration scheme have to be considered. A time integration scheme is called unconditionally stable, if the stability of the method does not depend on the time step length. Usually, explicit time integration methods are only conditionally stable. For linear structural behavior, established methods based on the Newmark scheme show an unconditionally stable behavior. For the non-linear structural behavior, unconditionally stable time integration schemes are still a topic of ongoing research .

Within this work, small numerical dissipation is applied to ensure the stability of the time integration scheme. Since this proved to be sufficient more elaborate energy conserving schemes could be omitted. Numerical dissipation occurs if the time integration scheme causes an error in computing the amplitude of a dynamic response. This effect is welcome in reducing the nonphysical so-called spurious higher frequency modes that are likely to occur in time integration methods for Finite Element Methods. For the lower frequency modes, which are of interest for the accuracy of the analysis, the influence of numerical dissipation has to be restricted.

In the scope of this work, the Generalized-α time integration scheme is used. Thereby, it is possible to control the dissipation on the spurious higher frequency modes and to minimise the dissipation in the lower frequency modes. Compared to the Newmark

method, the Generalized-α time integration scheme's advantage is to maintain second order accuracy, providing that the relevant parameters are chosen in an appropriate way.

As in the Newmark scheme, displacements $\mathbf{d}_{n+1}$ and the velocity $\dot{\mathbf{d}}_{n+1}$ at the end of time step $\Delta t = t_{n+1} - t_n$ can be approximated to:

$$\mathbf{d}_{n+1} = \mathbf{d}_n + \Delta t\, \dot{\mathbf{d}}_n + \Delta t^2 \left(\left(\frac{1}{2} - \beta \right) \ddot{\mathbf{d}}_n + \beta\, \ddot{\mathbf{d}}_{n+1} \right) \tag{2.61}$$

$$\dot{\mathbf{d}}_{n+1} = \dot{\mathbf{d}}_n + \Delta t \left((1-\gamma)\, \ddot{\mathbf{d}}_n + \gamma \ddot{\mathbf{d}}_{n+1} \right) \tag{2.62}$$

β and γ are the so-called Newmark parameters. Using the displacements $\mathbf{d}_{n+1}$ as primary variable, velocity $\dot{\mathbf{d}}_{n+1}$ and acceleration $\ddot{\mathbf{d}}_{n+1}$ can be found by transforming eq. 2.61 and eq. 2.62 to:

$$\dot{\mathbf{d}}_{n+1} = \frac{\gamma}{\beta \Delta t} (\mathbf{d}_{n+1} - \mathbf{d}_n) - \frac{\gamma - \beta}{\beta} \dot{\mathbf{d}}_n - \frac{\gamma - 2\beta}{2\beta} \Delta t \ddot{\mathbf{d}}_n \tag{2.63}$$

$$\ddot{\mathbf{d}}_{n+1} = \frac{1}{\beta \Delta t^2} (\mathbf{d}_{n+1} - \mathbf{d}_n) - \frac{1}{\beta \Delta t} \dot{\mathbf{d}}_n - \frac{1 - 2\beta}{2\beta} \ddot{\mathbf{d}}_n \tag{2.64}$$

For the Generalized-α method, two additional shift parameters α_m and α_f are introduced. In the time interval $[t_n, t_{n+1}]$, α_m and α_f are applied for interpolation:

$$\ddot{\mathbf{d}}_\alpha = (1-\alpha_m) \ddot{\mathbf{d}}_{n+1} + \alpha_m\, \ddot{\mathbf{d}}_n \tag{2.65}$$

$$\dot{\mathbf{d}}_\alpha = (1-\alpha_f) \dot{\mathbf{d}}_{n+1} + \alpha_f\, \dot{\mathbf{d}}_n \tag{2.66}$$

$$\mathbf{r}_\alpha^{int} = (1-\alpha_f) \mathbf{r}_{n+1}^{int} + \alpha_f\, \mathbf{r}_n^{int} \tag{2.67}$$

$$\mathbf{r}_\alpha^{ext} = (1-\alpha_f) \mathbf{r}_{n+1}^{ext} + \alpha_f\, \mathbf{r}_n^{ext} \tag{2.68}$$

Inserting eq. 2.61 and eq. 2.62 as well as eq. 2.65 -2.68 into the semi-discrete equation of motion eq. 2.59, the dynamic equilibrium can be formulated as:

$$\begin{aligned} \frac{1-\alpha_m}{\beta \Delta t^2} \mathrm{M} \ddot{\mathbf{d}}_{n+1} + (1-\alpha_f) \mathbf{r}_{n+1}^{int} = (1-\alpha_f) \mathbf{r}_{n+1}^{ext} + \alpha_f \mathbf{r}_n^{ext} - \alpha_f \mathbf{r}_n^{int} + \\ \mathrm{M} \left[\frac{1-\alpha_m}{\beta \Delta t^2} \ddot{\mathbf{d}}_n + \frac{1-\alpha_m}{\beta \Delta t} \dot{\mathbf{d}}_n + \left(\frac{1-\alpha_m}{2\beta} - 1 \right) \ddot{\mathbf{d}}_n \right] \end{aligned} \tag{2.69}$$

By the choice of the Newmark parameters β and γ and the interpolation parameters α_m and α_f, the degree of numerical dissipation is controlled. Depending on the spectral radius ρ_∞, the four parameters can be determined as:

$$\alpha_m = \frac{2\rho_\infty - 1}{\rho_\infty + 1} \qquad \alpha_f = \frac{\rho_\infty}{\rho_\infty + 1} \qquad \beta = \frac{1}{4}(1 - \alpha_m + \alpha_f)^2 \qquad \gamma = \frac{1}{2} - \alpha_m + \alpha_f \tag{2.70}$$

For the high frequency range, the numerical dissipation can be evaluated by the spectral radius $\rho_\infty \in [0,1]$. For ρ_∞=1 no numerical dissipation is applied, but the computation might face unstable behavior for nonlinear problems. A choice of ρ_∞ in the range of [0.85,0.95] introduces a numerical damping in the high frequency modes, which proved to be sufficient for the examples presented in the scope of this work. However, this method requires the time step to be small enough, so that relevant physical modes are not regarded as spurious and subject to numerical dissipation.

2.2.2.3 Linearisation

For the linearisation of the problem, eq. 2.69 is transformed into a residual form:

$$\begin{aligned} \mathrm{R}\left(\bar{\mathrm{d}}_{n+1}\right) = {} & \frac{1-\alpha_m}{\beta\Delta t^2}\mathrm{M}\bar{\mathrm{d}}_{n+1} + (1-\alpha_f)\mathrm{r}^{int}\left(\bar{\mathrm{d}}_{n+1}\right) - (1-\alpha_f)\mathrm{r}^{ext}_{n+1} - \\ & \alpha_f \mathrm{r}^{ext}_n + \alpha_f \mathrm{r}^{int}\left(\bar{\mathrm{d}}_n\right) - \mathrm{M}\left[\frac{1-\alpha_m}{\beta\Delta t^2}\bar{\mathrm{d}}_n + \frac{1-\alpha_m}{\beta\Delta t}\dot{\bar{\mathrm{d}}}_n + \left(\frac{1-\alpha_m}{2\beta} - 1\right)\ddot{\bar{\mathrm{d}}}_n\right] = 0 \end{aligned} \tag{2.71}$$

The solution is computed by a Newton-Raphson iteration. For the iteration, a new index *k* is introduced, which describes the number of the current iteration. For a specific time step *n*+1, starting from the last computed residuum vector $\mathbf{R}(\mathbf{d}^{-k})$, the new residuum vector $\mathbf{R}(\mathbf{d}^{-k+1})$shall be computed. For the linearisation the Taylor-series is used:

$$\mathrm{R}(\bar{\mathrm{d}}^{k+1}_{n+1}) = \mathrm{R}(\bar{\mathrm{d}}^{k}_{n+1}) + \frac{\partial \mathrm{R}(\bar{\mathrm{d}}^{k}_{n+1})}{\partial \bar{\mathrm{d}}_{n+1}}\Delta\bar{\mathrm{d}}^{k+1}_{n+1} + \mathcal{O}\left(\left(\Delta\bar{\mathrm{d}}^{k+1}_{n+1}\right)^2\right) = 0 \tag{2.72}$$

$$\text{with} \qquad \Delta\bar{\mathrm{d}}^{k+1}_{n+1} = \bar{\mathrm{d}}^{k+1}_{n+1} - \bar{\mathrm{d}}^{k}_{n+1} \tag{2.73}$$

By truncating the Taylor-series after the linear term, a linear system of equations is deduced:

$$\frac{\partial \mathrm{R}(\bar{\mathrm{d}}^{k}_{n+1})}{\partial \bar{\mathrm{d}}_{n+1}}\Delta\bar{\mathrm{d}}^{k+1}_{n+1} = -\mathrm{R}(\bar{\mathrm{d}}^{k}_{n+1}) \tag{2.74}$$

Inserting eq. 2.71 into eq. 2.74, the following equation is derived:

$$\left[\frac{1-\alpha_m}{\beta\Delta t^2}\mathrm{M}+(1-\alpha_f)\underbrace{\frac{\partial \mathrm{r}^{int}\left(\bar{\mathrm{d}}_{n+1}^{k}\right)}{\partial \bar{\mathrm{d}}_{n+1}}}_{\mathrm{K}_T}\right]\Delta\bar{\mathrm{d}}_{n+1}^{k+1}=$$
$$-\frac{1-\alpha_m}{\beta\Delta t^2}\mathrm{M}\bar{\mathrm{d}}_{n+1}^{k}-(1-\alpha_f)\mathrm{r}^{int}\left(\bar{\mathrm{d}}_{n+1}^{k}\right)+(1-\alpha_f)\mathrm{r}_{n+1}^{ext}$$
$$-\alpha_f\mathrm{r}_{n}^{ext}+\alpha_f\mathrm{r}^{int}\left(\bar{\mathrm{d}}_{n}\right)+\mathrm{M}\left[\frac{1-\alpha_m}{\beta\Delta t^2}\bar{\mathrm{d}}_{n}+\frac{1-\alpha_m}{\beta\Delta t}\dot{\bar{\mathrm{d}}}_{n}+\left(\frac{1-\alpha_m}{2\beta}-1\right)\ddot{\bar{\mathrm{d}}}_{n}\right] \qquad (2.75)$$

$\mathbf{K}_T(\bar{\mathbf{d}}_{n+1}^{k})$ is the tangential stiffness matrix after time step n+1 and iteration step k. The term in brackets on the left side of eq. 2.75 can be identified as the effective stiffness matrix K_T^{eff}

$$\mathrm{K}_T^{eff}(\bar{\mathrm{d}}_{n+1}^{k})=\left[\frac{1-\alpha_m}{\beta\Delta t^2}\mathrm{M}+(1-\alpha_f)\mathrm{K}_T\left(\bar{\mathrm{d}}_{n+1}^{k}\right)\right] \qquad (2.76)$$

and the term on the right side of eq. 2.75

$$\mathrm{r}^{eff}(\bar{\mathrm{d}}_{n+1}^{k},\bar{\mathrm{d}}_{n})=-\frac{1-\alpha_m}{\beta\Delta t^2}\mathrm{M}\bar{\mathrm{d}}_{n+1}^{k}-(1-\alpha_f)\mathrm{r}^{int}\left(\bar{\mathrm{d}}_{n+1}^{k}\right)+(1-\alpha_f)\mathrm{r}_{n+1}^{ext}+$$
$$\alpha_f\mathrm{r}_{n}^{ext}+\alpha_f\mathrm{r}^{int}\left(\bar{\mathrm{d}}_{n}\right)+\mathrm{M}\left[\frac{1-\alpha_m}{\beta\Delta t^2}\bar{\mathrm{d}}_{n}+\frac{1-\alpha_m}{\beta\Delta t}\dot{\bar{\mathrm{d}}}_{n}+\left(\frac{1-\alpha_m}{2\beta}-1\right)\ddot{\bar{\mathrm{d}}}_{n}\right] \qquad (2.77)$$

as the effective load vector. Using efficient stiffness and efficient load vector, the linearised nonlinear elastic problem is stated as:

$$\mathrm{K}_T^{eff}(\bar{\mathrm{d}}_{n+1}^{k})\,\Delta\bar{\mathrm{d}}_{n+1}^{k+1}=\mathrm{r}^{eff}(\bar{\mathrm{d}}_{n+1}^{k},\bar{\mathrm{d}}_{n}) \qquad (2.78)$$

Equation 2.78 is solved for $\Delta\bar{\mathbf{d}}_{n+1}^{k+1}$. The solution is used to update $\bar{\mathbf{d}}_{n+1}^{k}$ by applying eq. 2.73. For a converged solution it holds: $\bar{\mathbf{d}}_{n+1}^{k+1}\approx\bar{\mathbf{d}}_{n+1}^{k}$. Using a good initial predictor for this Newton scheme, quadratic convergence can be reached. Velocity $\dot{\bar{\mathbf{d}}}_{n}$ and acceleration $\ddot{\bar{\mathbf{d}}}_{n}$ at the beginning and end of a time step are derived based on eq. 2.61 and 2.62.

2.3 Modeling of Membrane Structures

2.3.1 Numerical Analysis of Structural Behavior of Membrane Structures

Membrane structures are classified as surface structures, since their ratio of thickness h to span L is usually $h/L<<1$. Each material point on the surface can be identified by two Gaussian surface parameters θ^1 and θ^2 at a certain time t in the current configuration $\mathbf{x}(\theta^1, \theta^2)$ and in the reference configuration $\mathbf{X}(\theta^1, \theta^2)$. Using these properties, the equations derived in section 2.2.1 can be simplified by an early semi-discretisation in thickness direction θ^3, while the other dimensions stay continuous. Furthermore, based on the spatial load carrying behavior of membranes, the following assumptions are introduced:

a The thickness of the membrane is considered as constant and comparably thin. In accordance with the behavior of available membrane material the Poisson effect in thickness direction is neglected.

b Normal stress is constant over the thickness.

c Only normal and in-plane shear stresses are acting in the mid plane. All stress and strain components with respect to the thickness direction are zero.

Due to the 'in advance' discretisation in thickness direction, the element wise contributions of virtual work in the spatially fully discretized system can be simplified for eq .2.44, eq. 2.49, and eq. 2.55 to:

$$\delta W^e_{dyn} = h \int_{A^e_0} \rho_0 \, \delta \mathrm{d}^h \cdot \ddot{\mathrm{d}}^h \, dA^e_0 \tag{2.79}$$

$$\delta W^e_{ext} = \int_{\Gamma^e_0} \hat{\mathrm{T}} \cdot \delta \mathrm{d}^h \, d\Gamma^e_0 + h \int_{A^e_0} \rho_0 \, \mathrm{B} \cdot \delta \mathrm{d}^h \, dA^e_0 \tag{2.80}$$

$$\delta W^e_{int} = h \int_{A^e_0} \delta \mathrm{E}^h : \mathrm{S}^h \, dA^e_0 \tag{2.81}$$

A_0^e is the area of a finite surface element in initial configuration. With spatial discretisation for all dimensions at a certain point in time t, the displacement $\mathbf{d}(\theta^1, \theta^2) = \mathbf{x}(\theta^1, \theta^2) - \mathbf{X}(\theta^1, \theta^2)$ and the virtual displacement $\delta\mathbf{d}(\theta^1, \theta^2)$ for a material point can be approximated as:

$$\mathrm{d}(\theta^1, \theta^2) = \sum_{i=1}^{n_{nod}} N_i(\theta^1, \theta^2) \cdot \bar{\mathrm{d}}_i \tag{2.82}$$

$$\delta\mathrm{d}(\theta^1, \theta^2) = \sum_{i=1}^{n_{nod}} N_i(\theta^1, \theta^2) \cdot \delta\bar{\mathrm{d}}_i \tag{2.83}$$

This holds for the time derivative of the displacement vector $\delta\mathbf{d}(\theta^1, \theta^2)$, the velocity vector $\delta\dot{\mathbf{d}}(\theta^1, \theta^2)$, and the acceleration vector $\delta\ddot{\mathbf{d}}(\theta^1, \theta^2)$, respectively. All stress components normal to the surface are zero, i.e.:

$$S^{i3}=S^{3i}=0 \text{ and } \sigma^{i3}=\sigma^{3i}=0 \qquad (2.84)$$

The strain state can be derived via the strain tensor of the mid surface:

$$\mathrm{E} = \frac{1}{2}(g_{\alpha\beta} - G_{\alpha\beta})\mathrm{G}^{\alpha} \otimes \mathrm{G}^{\beta} \qquad (2.85)$$

The artificially imposed prestress is taken into account as a residual stress added to the elastic stress in the reference configuration. The resulting PK2 stress tensor **S** in reference configuration is the sum of the prestress tensor $\mathbf{S}_{pre}$ and the elastic stress tensor $\mathbf{S}_{el}$:

$$\mathbf{S} = \mathbf{S}_{pre} + \mathbf{S}_{el} = \mathbf{S}_{pre} + \mathrm{C}: \mathbf{E} \qquad (2.86)$$

For the usage of foils, an isotropic material behavior can be assumed. Accordingly, the components of the material tensor **C** can be derived as:

$$C^{\alpha\beta\gamma\delta} = \overline{\lambda} G^{\alpha\beta} G^{\gamma\delta} + \mu(G^{\alpha\gamma} G^{\beta\delta} + G^{\alpha\delta} G^{\beta\gamma}) \qquad (2.87)$$

$$\text{with} \quad \overline{\lambda} = \frac{2\lambda\mu}{\lambda + 2\mu} = \frac{E\nu}{1 - \nu^2} \quad \text{and} \quad \mu = \frac{E}{2(1+\nu)} \qquad (2.88)$$

Fabrics initially show an anisotropic, mainly orthotropic behavior in the perpendicular directions of warp and weft. Furthermore, fabrics feature non-elastic, time and load history dependent properties.

The procedures for time discretisation and the linearisation of membrane and cable elements are derived according to those presented in section 2.2.2.2 and section 2.2.2.3.

For the discretisation of edge cables, a cable element formulation can be derived by introducing a second early spatial discretisation. All stress components perpendicular to the cable axis vanish and the cross section features a constant stress distribution.

2.3.2 Form Finding

Already in their initial state, membrane structures are subject to dead load and prestress. As explained above, the geometry of the structure has to ensure an equilibrium of internal membrane forces (including those due to prestress) and loadings. Therefore, the initial ge-

ometry of a membrane structure cannot be easily derived, but is the result of experimental or numerical analysis. The resulting shape resembles a free form surface, which generally cannot be generated by analytical methods.

The procedure of deriving the initial shape of a membrane structure is called **form finding**. As the form finding procedure is a both essential and challenging task in the design of membrane structures, fundamental equations and solution methods are introduced in the following sections.

In a classical structural analysis, deformation and stress of a structure are computed based on the known geometry, the known load conditions, and material parameters. In contrast, the aim of a form finding procedure is to find a geometry for which a certain internal stress state and, in case, an external loading state, are in equilibrium. Additionally, the geometry has to satisfy prescribed geometric boundary conditions. As the geometry is the unknown while the internal and external stress distributions are prescribed, form finding can be identified as an inverse problem.

In experimental approaches, small scale models are used to simulate a certain stress distribution in a flexible material and to record the resulting shapes. If a shape satisfies all requirements, it is upscaled and used as initial geometry for further design processes. Rubber, thin fabrics, or soap films are used as materials in the small scale models.

In a numerical approach, the inverse problem of form finding is solved by computations. An arbitrary initial geometry, which satisfies the geometric boundary conditions, such as placement and type of supports, is chosen. This geometry serves as a known reference configuration (see fig. 2.5(a)). The aim is to derive a new geometry as current configuration, which is in equilibrium for a prescribed prestress state (see fig. 2.5(b). In the following section, the problematic and solution strategies for a numerical form finding are introduced.

2.3.2.1 Numerical Form Finding

In the following a mechanically prestressed structure is assumed. For form finding considerations, the low self-weight of the membrane itself has little influence on the result compared to the prestress. Therefore, it is neglected as well as all external loads. Performing the form finding procedure without any loading but prestress, the geometry of the membrane solemnly depends on the distribution of membrane prestress and, in case, the ratio to prestress of edge cables. In the design process this fact is utilised. Firstly, the distribution of prestress in the different structural elements is adjusted to derive an acceptable shape. Secondly, while keeping the prestress distribution constant, the level of the prestress is adjusted according to further requirements, such as the capability to withstand design loads.

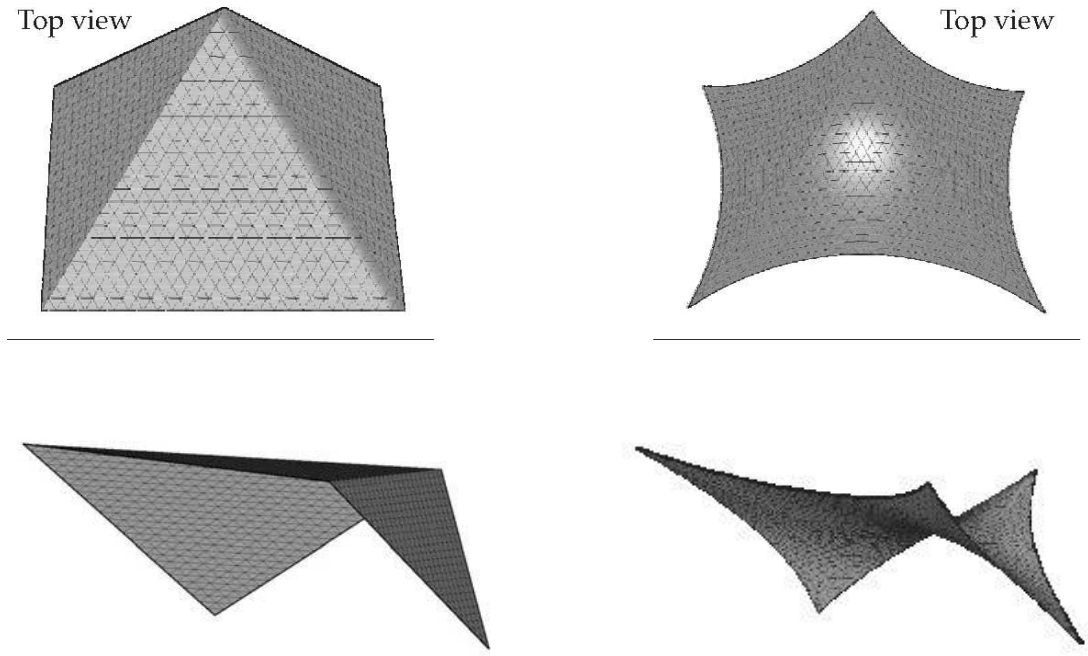

(a) Arbitary initial shape (reference configuration)

(b) Resulting equilibrium shape (current configuration)

Figure 2.5: Form finding computation

The state of equilibrium of the internal forces in the membrane can be described by the principle of virtual work in the integral (weak) sense:

$$\delta W_\sigma = h \int_a \sigma : \delta \mathrm{d}_{,\mathbf{x}} \, da = 0 \qquad (2.89)$$

This resembles the state of equilibrium in the current configuration **x**, with σas the Cauchy stress tensor and $a$as the area of the membrane surface. The displacement vector **d** describes the change of geometry from reference to current configuration, from the assumed initial geometry to the aspired "geometry of equilibrium". $\mathbf{d}_{,x}$ is the derivative of the displacement vector with respect to the current configuration.

The state of equilibrium can be described in the reference configuration **X** equivalently:

$$\delta W_S = h \int_A (\mathrm{F} \cdot \mathrm{S}) : \delta \mathrm{F}\, dA = 0 \qquad (2.90)$$

with **S** as the second Piola-Kirchhoff stress tensor and A as the area of the membrane surface of the reference configuration. The deformation gradient **F** connects the reference configuration to the current configuration:

$$d\mathbf{x} = \mathbf{F} \cdot d\mathbf{X} \qquad (2.91)$$

Using the deformation gradient together with further rearrangement, the principle of virtual work in the current configuration can be transformed to:

$$\delta W_\sigma = h \int_A det\mathrm{F}\, (\sigma \cdot \mathrm{F}^{-T}) \; : \; \delta \mathrm{F}\, dA = 0 \qquad (2.92)$$

In the general case, no analytical solution is possible. The Finite Element Method is used to solve the problem in a point wise manner for a discretised geometry. The translational degrees of freedom of the nodes of the finite element mesh are chosen as variables. Using the iso-parametric concept, the discretised geometry $x^h(\theta^1, \theta^2)$ and displacement $d^h(\theta^1, \theta^2)$ of the structure are approximated based on the position of the nodes of the finite element mesh via the shape functions:

$$x^h(\theta^1, \theta^2) = \sum_{k=1}^{n_{nod}} N_k(\theta^1, \theta^2) \cdot \overline{\mathbf{x}}_k \qquad (2.93)$$

$$d^h(\theta^1, \theta^2) = \sum_{k=1}^{n_{nod}} N_k(\theta^1, \theta^2) \cdot \bar{\mathbf{d}}_k \qquad (2.94)$$

In a Cartesian coordinate system with orthogonal basis $\mathbf{e}_i$, the position $\mathbf{x}_k$ and displacement $\bar{\mathbf{d}}_k$ of a node k can be determined by the their coefficients x_k^i and d_k^i:

$$\overline{\mathbf{x}}_k = x_k^1 \mathbf{e}_1 + x_k^2 \mathbf{e}_2 + x_k^3 \mathbf{e}_3 \qquad (2.95)$$

$$\bar{\mathbf{d}}_k = d_k^1 \mathbf{e}_1 + d_k^2 \mathbf{e}_2 + d_k^3 \mathbf{e}_3 \qquad (2.96)$$

The unknown

coefficients of the nodal displacements d^i_k are identified as unknowns of the form finding computation. They are summarised into a vector **b** of size n_{dof}, whose components b_r resemble the r-th degree of freedom of the discretized problem. Using the fundamental lemma of variational calculus and the vector of unknowns b_r, the following nonlinear system of equations with n_{dof} equations can be derived:

$$\frac{\partial W_\sigma}{\partial b_r} = h \int_A det\mathrm{F}\,(\boldsymbol{\sigma} \cdot \mathrm{F}^{-T}) \;:\; \frac{\partial \mathrm{F}}{\partial b_r}\, dA = 0 \quad \forall\, r \in [1, n_{\mathrm{dof}}] \tag{2.97}$$

For the linearisation of eq. 2.97 similar procedures to those described in section 2.2.2.1 are applied for the membrane and cable elements introduced in section 2.3.1 . Following the common procedure of geometrically nonlinear structural analysis, a direct solution via an iterative Newton-Raphson iteration seems to be possible.

2.3.2.2 Solving the Inverse Problem

Typically, inverse problems are ill posed in contrast to well posed problems, where a known physical situation is modeled. According to the French mathematician Jacques Hadamard (*1865, †1963), a well posed problem is defined by the properties of existence, uniqueness and stability of its solution. Ill-posed problems usually need to be re-formulated for numerical treatment. Typically this involves including additional assumptions. This process is known as regularisation.

Form finding is an ill-posed problem. Especially the non-uniqueness of the solution can be easily explained: An identical surface can be approximated by different sets of nodal co-ordinates for a finite element discretisation (fig. 2.6). This is due to the fact that except for the nodes at the edge, the FE-based nodes can move tangentially to the surface without this movement causing any strain energy. Therefore, the stiffness matrix of the system is singular for tangential movements within the membrane surface. Thus, eq. 2.97 is not solvable in a standard computation. A restriction of the degrees of freedom for the form finding computation to those perpendicular to the membrane surface would enable a simple solution, but is not applicable, since e.g. for flexible cable support, the possibility of tangential movements is necessary for a realistic physical modeling.

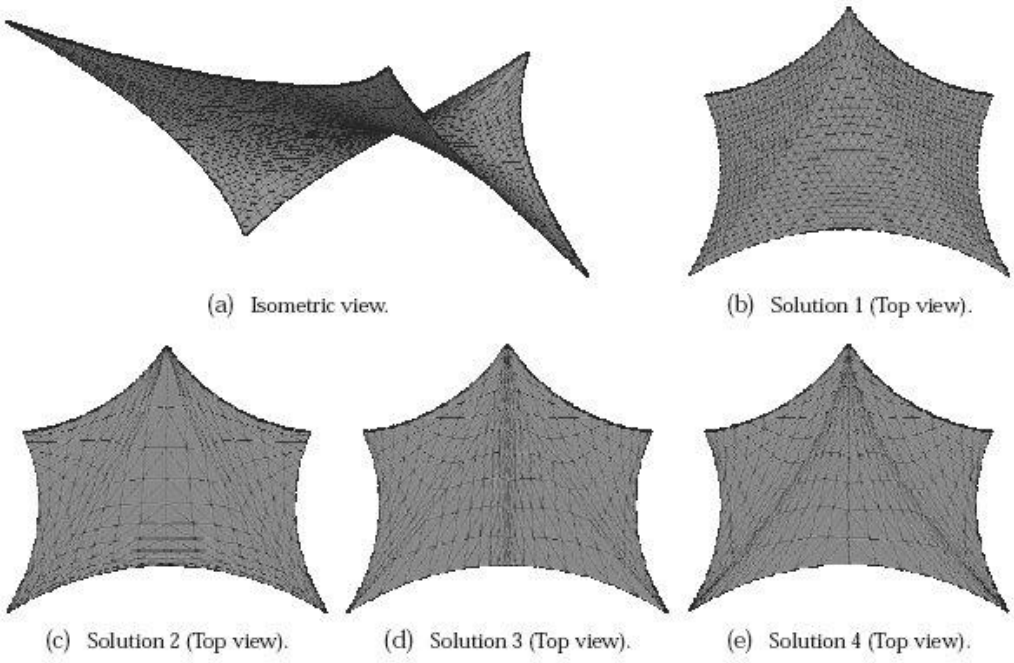

Figure 2.6: Multiple valid solutions for a form finding problem.

Several methods have been developed to overcome the difficulties of the inverse form finding problem. In the following, the basic ideas of the most common methods are presented:

a **Modified linearisation of the problem**

For the Newton-Raphson type iterative solution of the discretised problem, a not consistently derived, non-singular stiffness matrix is used to approximate the problem.

b **Dynamic Relaxation**

Applying dynamic relaxation, the steady-state form finding problem is transferred into a dynamic problem by adding inertia and damping effects to the system. Thereby, the initially ill-posed problem becomes well-posed. The process of form finding is modeled as decay of an oscillation. The quiescent state serves as resulting geometry of the form finding computation .

c **Homotopy methods**

General mathematical methods to approach a solution of a singular problem are methods of numerical continuation , also called homotopy methods . A homotopy is a continuous transformation of one function into another. The basic idea to use homotopy in form finding is to modify the originally singular problem by a related well defined one, which fades out as the solution is approached. As an example, a singular problem $f(x)=0$ is modified by a non-singular problem $g(x)=0$ to the homotopy $h(x)=0$ with the homotopy factor $\lambda \in [0;1]$:

$$h(x) = \lambda f(x) + (1 - \lambda) g(x) = 0 \tag{2.98}$$

The solution of $h(x)=0$ approaches the solution of $f(x)=0$ for λ approaching 1. The method

is more successful as the function $g(x)=0$ is closer to the original function $f(x)=0$. Applied to the problem of form finding, the original singular function is the formulation of virtual work in the current configuration: $\delta W_\sigma=0$. The related non-singular function is the formulation of virtual work in the reference configuration with prescribed PK2 stress: $\delta W_S=0$.

$$\begin{aligned} \delta W_\lambda &= \lambda \delta W_\sigma + (1-\lambda)\delta W_S \\ &= \lambda h \int_A det\mathrm{F}\,(\sigma \cdot \mathrm{F}^{-T}) : \delta \mathrm{F}\, dA + (1-\lambda) h \int_A (\mathrm{F} \cdot \mathrm{S}) : \delta \mathrm{F}\, dA = 0 \end{aligned} \qquad (2.99)$$

The stabilising effect of δW_S is due to the constant and known reference configuration, for which the PK2 stress is prescribed. By increasing λ from 0 to 1 until the solution fails, the geometry derived by the modified problem can be taken as an approximate solution of the original problem. The closer the homotopy factor λ is to 1, the closer the solution of the modified problem is to the solution of the original problem.

Another important property of eq. 2.99 is that the closer the reference configuration is to the current configuration, the better the stabilisation term δW_S describes the original problem. This property is used in the Updated Reference Strategy.

– Updated Reference Strategy (URS)

The Updated Reference Strategy was developed by Bletzinger and uses homotopy introduced above in an iterative manner. The solution of the modified problem (eq. 2.99) is used as reference configuration for the next iteration step. For each iteration step, the desired Cauchy stress σ and second Piola-Kirchhoff stress $\mathbf{S}$ are newly prescribed. The update of the reference configuration by the solution of the modified problem gives the Updated Reference Strategy its name.

With each iteration step, the difference between reference and current configuration decreases and the stabilisation term δW_S more accurately describes the original problem. Convergence is reached, if the difference between reference and the current configuration is smaller than a certain threshold. For this solution, $\sigma=\mathbf{S}$ and the solution of the modified problem is identical to the solution of the original problem. The convergence is independent of the value of the homotopy factor λ, as long as λ is small enough to enable the solution of the modified problem. For a small homotopy factor, the solution procedure is more robust but needs more iterations. For a larger choice of λ, less iteration steps are needed, as long as the solution of the modified problem is possible. In order to increase the performance of the form finding procedure, λ can be increased during the computation.

– **Force Density Method**

Initially, the Force Density Method was developed for the design of cable net constructions for the Olympic Stadium in Munich, Germany . Meanwhile it has been extended for the application of membrane structures . The singular original problem is modified by assuming a constant force density. With this modification, the problem is well-posed and can be solved. In an iterative manner, the solution is

used as a new reference configuration . The force density can be interpreted as a constant PK2 stress. Accordingly, the Force Density Method is a special form of the URS for λ=0. Only the stabilisation term δW_S=0 is solved as the modified problem. Therefore, the force density method appears to be a consistent part of the more general URS.

2.4 Example: The Leeming Awning Mobile Canopy Shelter

The structural model of the Leeming Awning has to incorporate form finding and non-linear analysis.

2.4.1 Initial Considerations

The canopy structure gains its stiffness from the anticlastic prestressed membrane, which is supported by eight tensioned cables and five steel support poles. The prestress is induced into the membrane by the cables. The support poles are standard scaffolding poles (54.5mm dia steel tube id 49.5mm) one is articulated at ground level and tensioned by another cable.

Large displacements of the membrane and the support poles are to be expected. Therefore, the numerical model of the Leeming Awning has to take into account non-linear kinematics. This necessitates a geometrically non-linear analysis. As only small to moderate strains and stresses are expected, a linear elastic material law is applied.

Inherent to geometrically non-linear structural analysis is the load-path dependency of the solution: for multiple load states, the structural deformation and stress state depend on the order in which the load states are applied. Thus, a load superposition is not sufficient for the consideration of multiple load cases. The application of prestress by tensing the respective cables, can be interpreted as an initial load case "prestress". The aim is to find a prestressed shape for the membrane with a uniform stress distribution. This is achieved by a form finding computation.

The setup of an exact prestressed structural model of the Leeming Awning requires detailed information about geometry and stress states. The bounding geometry was determined by a site survey which identified certain portions of the adjoining structure (the Leeming house) that could not be used due to its great age (>200 years) and flint and crumbling lime mortar construction. Detailed data about the initial stress state of the prestressed structural members, in general, and the membrane, in particular, is limited. It was determined that the program K3-Tent developed and made available for non-commercial use by Nizhny Novgorod State University, Russia provides an excellent first appoximation to the final stable form.

2.4.2 Form Finding Computation

The geometry and topology of the Leeming Awning was input into the K3-Tent program, taking account of the site restrictions. The result is shown as the "form found" mesh shown in figure 2.7.

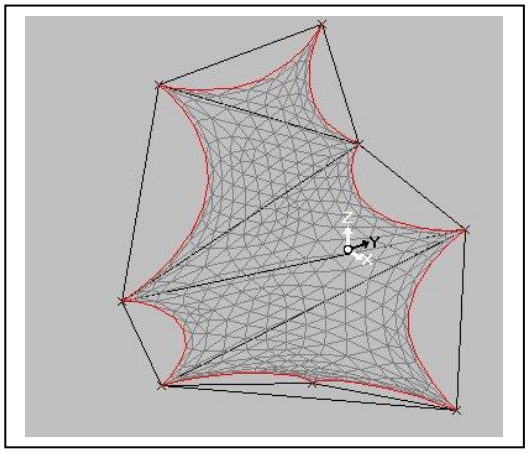

Figure 2.7 K3-Tent output

It was found that when transferred to the FEA program Ansys that there were significant geometrical errors, so the shape was corrected within the CAD program CATIA, and the corrected form is shown in Figure 2.8, and located within the full FEA model in Fig 2.9

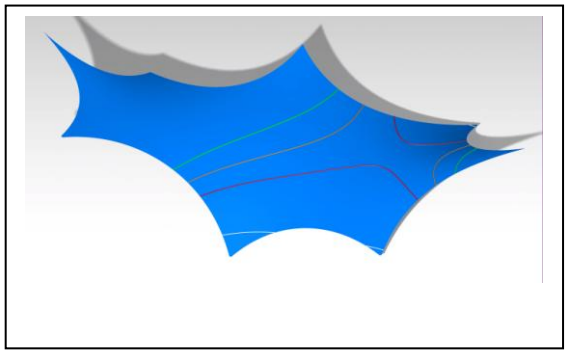

Figure 2.8 Geometrically corrected shape

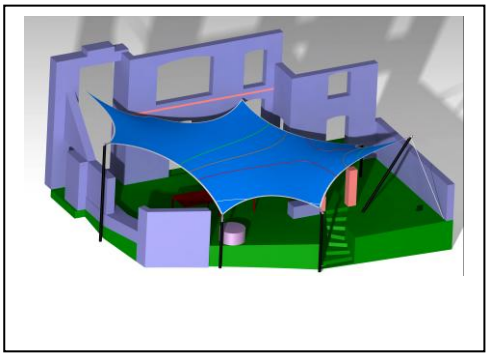

Figure 2.9 Awning within full FEA model

The plan view of the site is shown in figure 2.10

Figure 2.10 Model Plan view

At this stage it was confirmed that the final design would provide sufficient headroom and this is shown by the height contours in fig. 2.8, (red = 2 metres headroom).

The model was then tested within the Ansys environment using SHELL181 elements using the mesh shown in Figure 2.11

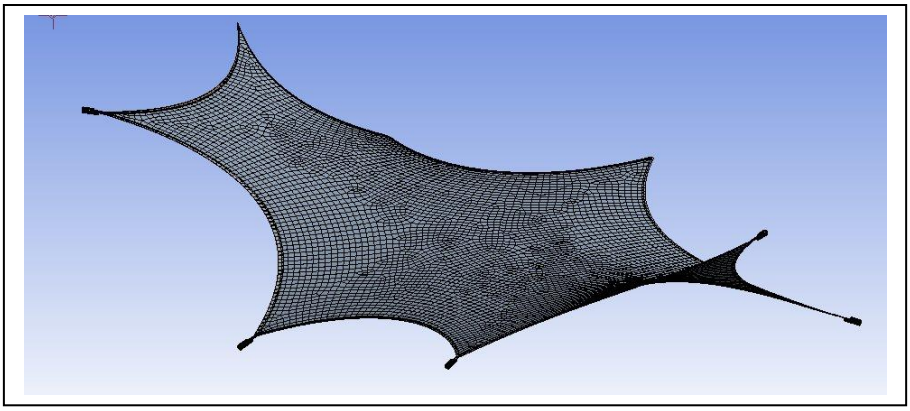

Figure 2.11
FEA mesh

It was also confirmed that the membrane could be flattened so that multiple strips of cloth could be sewn together to make the final Awning. Figure 2.12a,b,c,d,e show that the distortion from the final shape to a flat shape is less that 1 Degrees over the majority of the membrane, when it is split into 5 separate strips. 1 Degree should be easily absorbed by tensioning on the tensioning ropes.

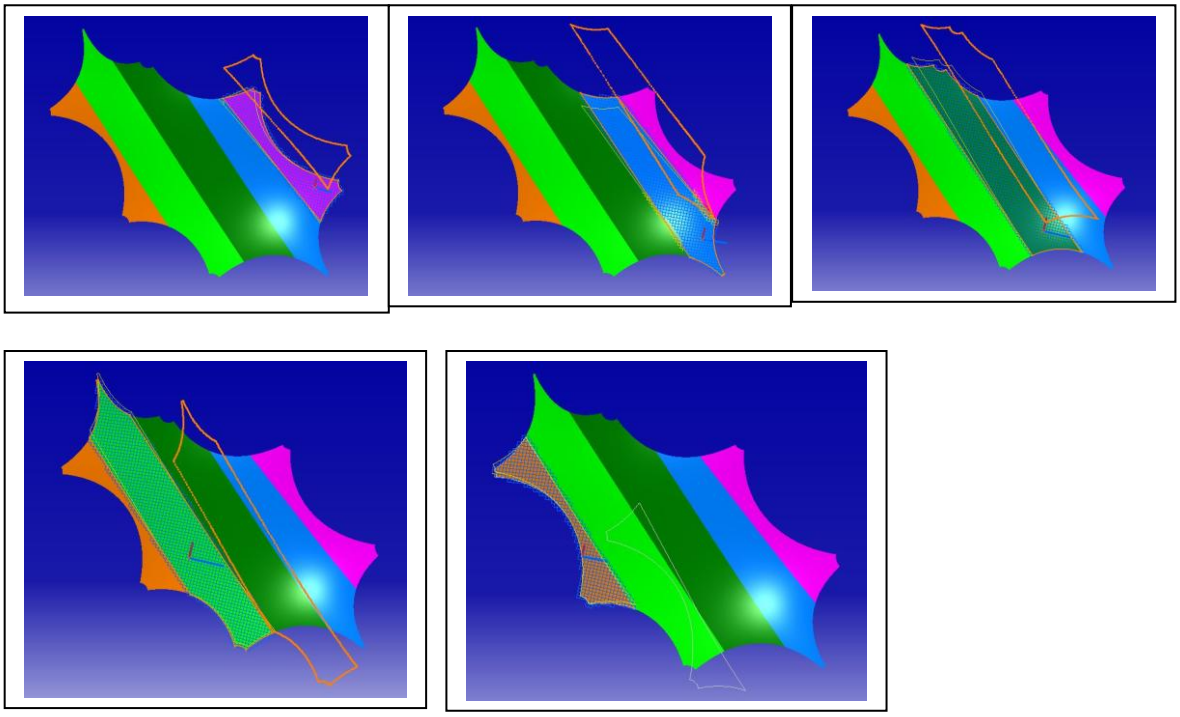

Figure 2.12a,b,c,d,e Flattening Blue = no distortion yellow = 1 Degree distortion

2.4.3 Analysis

The model of the Leeming Awning was subjected to non-linear structural behavior analysis. Whilst it was not possible to obtain unconditionally stable time integration solutions when self weight due to gravity effects on the awning, it did prove possible to obtain convergent solutions with self-weight omitted. Since the ripstop nylon fabric chosen has a weight of 68 grams / metre squared ignoring this addition to the stresses on the awning will have a negligible impact on the solution. Two cases were considered one of 16 Newtons of force applied at five points and one to investigate safety factors where 3000 Newtons were applied to the five points. The forces are shown in figures 2.13 and 2.14.

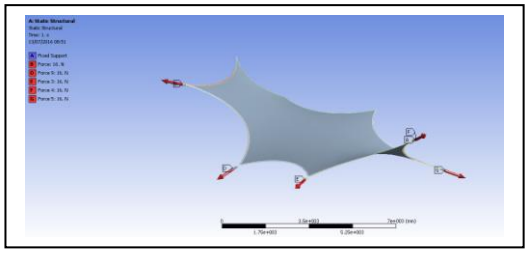

Figure 2.13 16 Newtons Loading

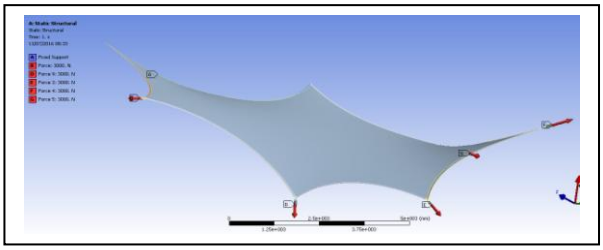

Figure 2.14 3000 Newtons Loading

The resulting displacements for the two case are shown in figures 2.15 and 2.16, from which it can be seen that the predicted displacements are less than 7mm worst case.

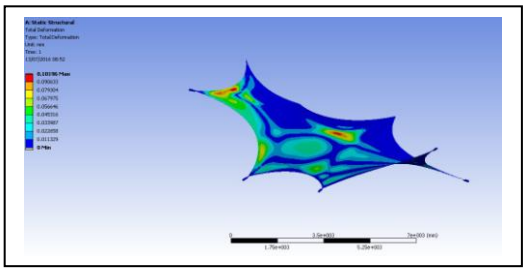

Figure 2.15 Displacement 16 Newton Loading

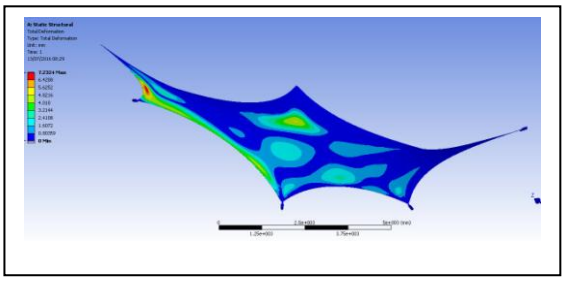

Figure 2.16 Displacement 3000 Newton Loading

The stresses are shown in figures 2.17 and 2.18, from which it can be seen that the normal stresses are a maximum of .26Mpa. Under the worst case scenario the stresses are a maximum of 58.6 Mpa primarily concentrated close to the awning attachment points.

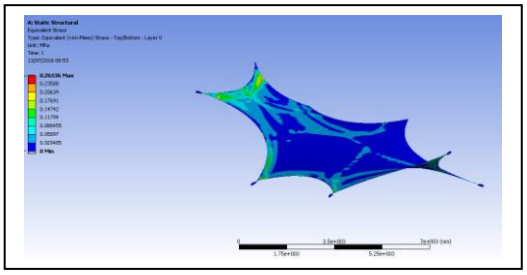

Figure 2.16 Stress 16 Newtons Loading

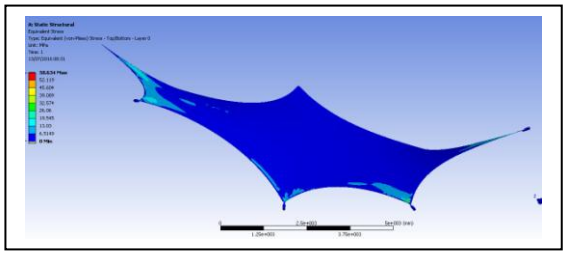

Figure 2.17 Stress 3000 Newtons Loading

In the case of the 3000 Newtons Loading the safety factor for the awning was calculated and is shown in figure 2.18, and gives just over a factor of 4, again primarily at the attach points. It is not considered that this load will be approached, but if this were to be the case then strengthening at the corners is indicated, probably by doubling the thickness of the awning for 0.5 metre from the corners.

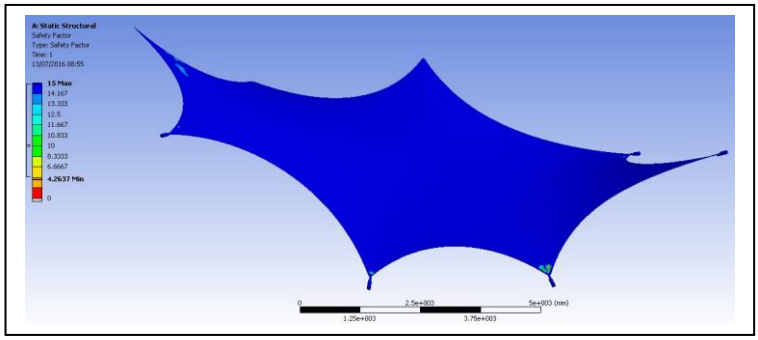

Figure 2.18 Safety factor 3000 Newtons Loading.

In order to check the flattenings (figures 12a-e) a 1 to 20 scale model was produced (Fig. 2.19), which confirmed that the structure was indeed stable, in accordance with the predictions of the K3-Tent software.

Figure 2.19 1 to 20 scale model of the Leeming Awning

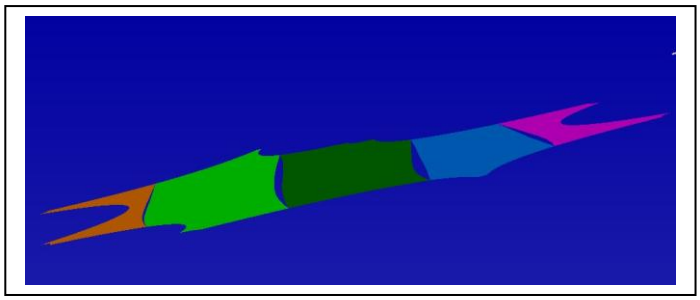

Figure 2.20 Five Flattening strips

Following this check the five flattening strips (an end-on view is shown in figure 2.20) were converted to Autocad .dxf format to be transferred to the specialist ripstop nylon fabricator for scaling up to fit the 150cm width material roll. The curved edges to the flattenings can be clearly seen in figure 2.20. However it was then discovered that ripstop nylon was only available in 150mm width rolls and the design in figure 2.20 required a roll width of about 180mm, so the positioning of the splitting lines in the awning was adjusted to that in figure 2.21, and a final scale model to check the design was produced as shown in figure 2.22.

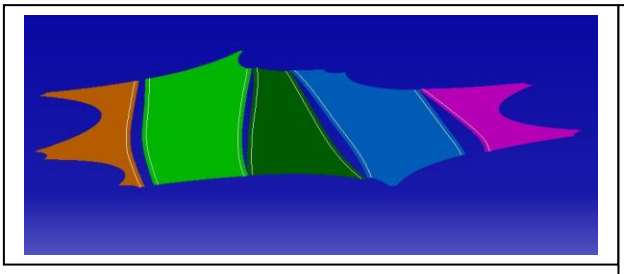

Figure 2.21 Flattened Strips 150mm fabric

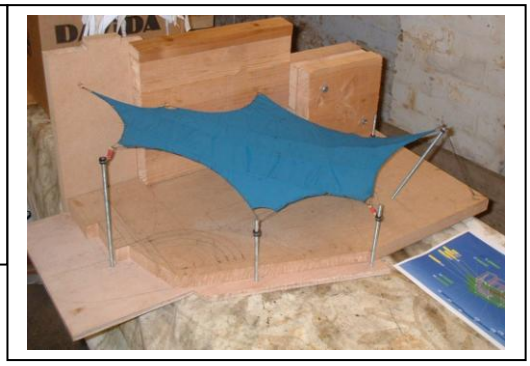

Figure 2.22 Final Model 5 strips

Positioning of the supports is shown in figure 2.23

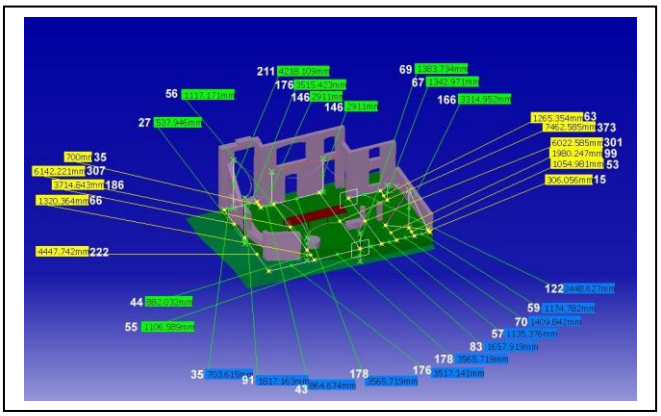

Figure 2.23 Positioning of the supports for the Leeming Awning

2.5 Wind Loading

This work was done using CFD numeric analysis. Initial work was done modelling the response of the awning to a uniform 20m/s wind, the standard for Oxfordshire for 1 in 50 chance of excess. (BSEN 1991-1-4:2005 + Al:2010 Incorporating National Amend1ment No.1 Figure NA.l Value of fundamental basic wind velocity v_b). This showed that in the worst case (northerly wind) there was an area of lower pressure above the awning near the supporting wall, see figure 2.24

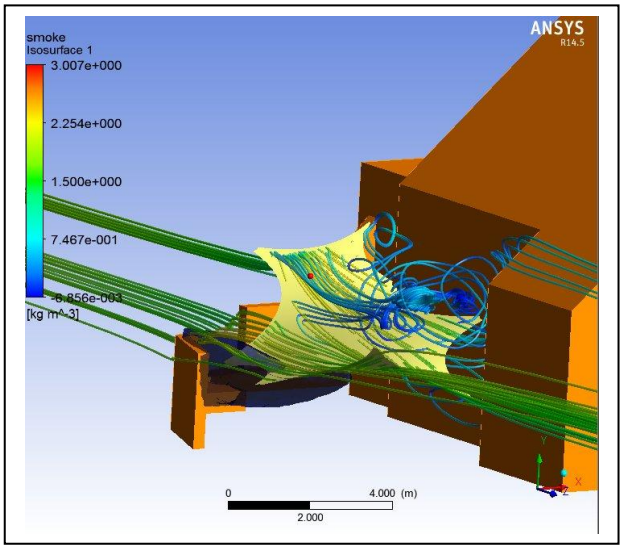

Figure 2.24 20m/s wind path.

This gave rise to the pressure distribution shown in figure 2.25

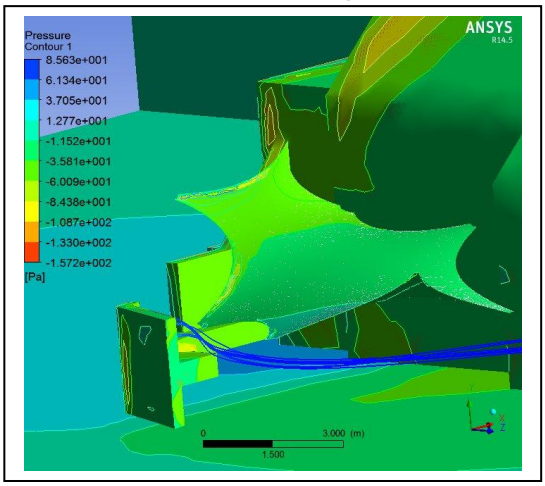

Figure 2.25 20m/s pressure distribution

However, further examination of the literature showed that the peak velocities are greater than the average value, but that the factor was no more than 1.7 worst case, so a figure of 2.0 was taken and further modelling was accordingly done at 40m/s. The results are shown in figure 2.26 and 2.27

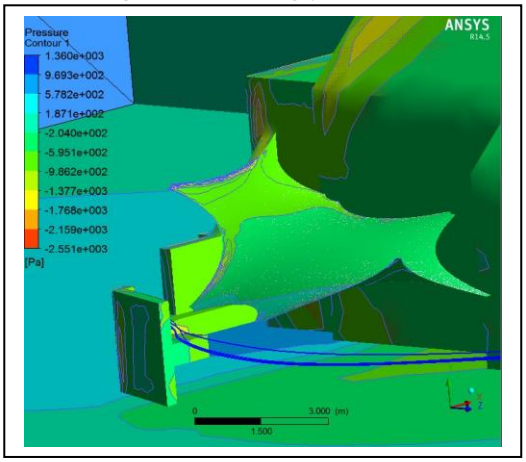

Figure 2.26 40m/s pressure distribution. ISO

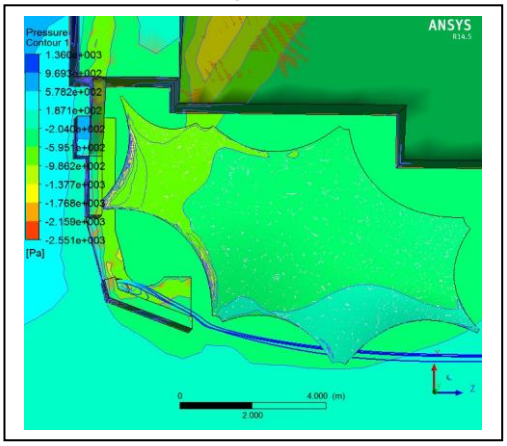

Figure 2.27 40m/s pressure distribution vertical

From this it can be seen that the greatest pressures are to be found on the leading edge of the awning. Isocontour of the topside and underside pressures are shown in figures 2.28 and 2.29

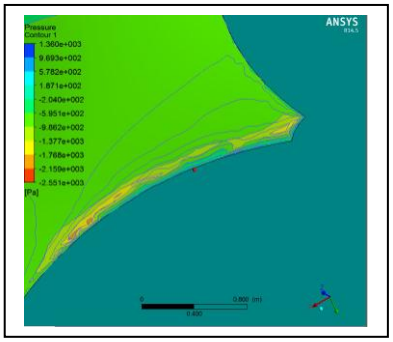

Figure 2.28 Detail pressure 40m/s Topside

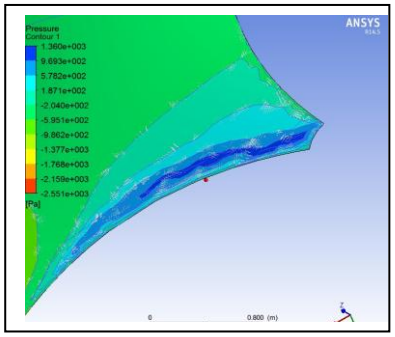

Figure 2.29 Detail pressure 40m/s Underside

Examination of these figures show that the worst case pressure differential is about half way along the top edge. The pressure field on the awning was exported from Ansys CFX and imported into Ansys Structural as an external load, as shown in figure 2.30

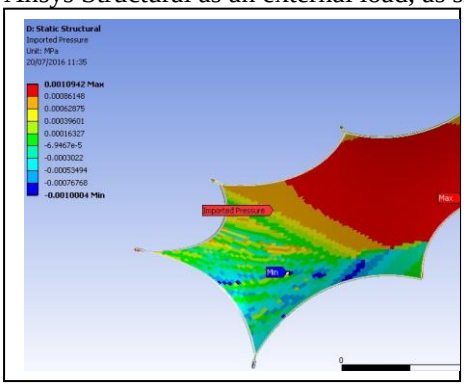

Figure 2.30 40 m/s pressure field

From this field it can be seen that the maximum pressure is 1094 Pa near to the lounge and -1000 Pa near to the gate posts. When the solver was run again this gave a maximum displacement for a polyester awning of about 1mm, see figure 2.31

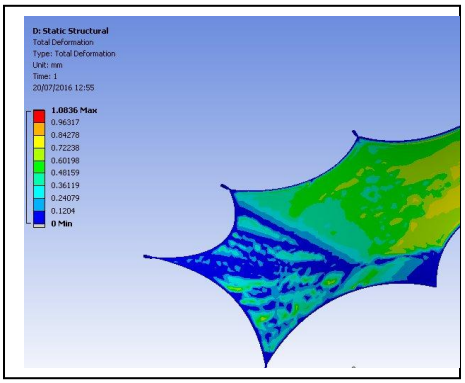

Figure 2.31 Displacement of awning in 40 m/s north wind

2.6 Conclusion

Whatever.